Using Extended Light Sources for Modeling Object Appearance under Varying Illumination

Imari Sato
National Institute of Informatics
imarik@nii.ac.jp

Takahiro Okabe   Yoichi Sato   Katsushi Ikeuchi
The University of Tokyo
{takahiro,ysato,ki}@iis.u-tokyo.ac.jp

Abstract

In this study, we demonstrate the effectiveness of using extended light sources for modeling the appearance of an object for varying illumination. Extended light sources have a radiance distribution that is similar to that of the Gaussian function and have the potential of functioning as a low-pass filter when the appearance of an object is sampled under them. This enables us to obtain a set of basis images of an object for variable illumination from input images of the object taken under those light sources without suffering aliasing caused by insufficient sampling of its appearance. Furthermore, extended light sources are useful in terms of reducing high contrast in image intensities due to specular and diffuse reflection components. This helps us observe both specular and diffuse reflection components of an object in the same image taken with a single shutter speed. We have tested our proposed approach based on extended light sources with objects of complex appearance that are generally difficult to model using image-based modeling techniques.

1. Introduction

The appearance of an object greatly changes depending on its surface reflectance properties and the lighting conditions of the location where the object is placed. For the task of object recognition and image synthesis, it is thus important to be able to predict the variation of an object appearance under varying illumination conditions. In this paper we investigate the effectiveness of using extended light sources for modeling the appearance of an object under varying illumination.

While there may seem to be a large variety of possible appearances for a given object, it has been demonstrated in previous research that the appearance changes of an object for varying illumination can be represented with a linear subspace spanned by a set of basis images of the object. For instance, in the case of a convex Lambertian object, its appearance seen under distant illumination without attached and cast shadows can be described with a 3-D linear subspace spanned from three input images of the object taken under linearly independent lighting conditions [10, 20, 25]. Even taking into account attached shadows, most of the image variation of a human face or other object under vary-

Real Image
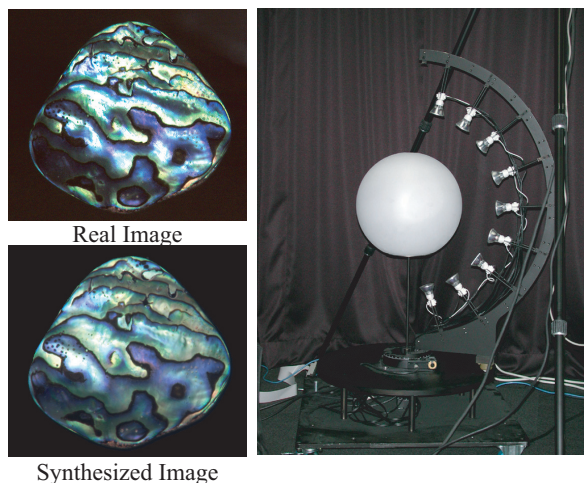
Synthesized Image

Figure 1. Synthesized appearance modeled by extended light sources.

ing illumination was shown to be adequately represented by a low-dimensional linear subspace slightly higher than 3-D [6, 3, 24]. A similar observation was utilized for object recognition in [4, 5].

A set of basis images spanning such a linear subspace are often provided by applying principal-component analysis to the input images of an object taken under different lighting conditions.[1] Since little is known about how to sample the appearance of an object in order to obtain its basis images correctly, a large number of input images taken by moving a point light source along a sphere surrounding the object are generally provided. Then the question is whether the use of a point light source is suitable for capturing the variation of the object's appearance. As one solution to this problem, Shim and Chen introduced a statistical approach that used training scenes with different shapes and surface materials for finding the most efficient lighting patterns to model the appearance changes of an object [19].

Recent investigations in frequency-space analysis of reflection have shown that the appearance of an object under varying complex illumination conditions can be well repre-

---

[1]In the context of texture synthesis, Malzbender et al. took an alternative approach of modeling the luminance dependencies of a texture on lighting directions with biquadratic polynomials [8].

sented with a linear subspace spanned by basis images of the object, called *harmonic images*, each of which corresponds to an image of the object illuminated under *harmonic lights* whose distributions are specified in terms of spherical harmonics [14, 15, 1].[2] Hence if harmonic lights can be physically constructed in a real setting, harmonic images of a real object can be obtained simply as images of the object seen under these light sources. However, harmonic lights are complex diffuse light sources comprising both negative and positive radiance and are thus difficult to physically construct in a real setting. Therefore, most of the previously proposed techniques synthetically compute harmonic images from the knowledge of an object 3-D shape and reflectance properties.

Lee et al. introduced the interesting concept of object classes for determining a configuration of nine light source directions. Input images taken under those particular light source directions approximate a 9-D subspace spanned by harmonic images [7]. This method has the advantage that it requires only synthetically provided harmonic images for one object in each class in order to determine the nine lighting directions.

Recently, we introduced a method incorporating the sampling theorem of spherical harmonics for determining a set of lighting directions to efficiently sample the appearance of an object using point light sources [17]. The sampling theorem specifies how to substitute a set of realizable light sources for harmonic lights, and harmonic images of the object are computed as weighted sums of the sampled appearance of the object under those point light sources. While this method does not require knowledge about the 3-D shape and reflectance properties of an object, information about the highest frequency that the appearance of an object contains must be provided in order to determine the number of point light sources required. How to provide such information for a given object remains unsolved.

The sampling theorem states that the higher the frequency content of an object's appearance, the more input images are required to obtain a correct set of basis images. The number of input images required may become extremely large in the case of highly specular surfaces containing a large quantity of high frequency components in their reflection. In this case, insufficient sampling of an object appearance will result in aliasing in the basis images, and this will lead to undesirable artifacts in the synthesized appearance.

Since the number of input images provided for modeling an object's appearance is usually limited, an anti-aliasing framework for obtaining a set of correct basis images from an insufficient number of object input images is needed. However, this aliasing problem has not been carefully considered in previous studies.

In this study, we propose a novel approach for sampling the appearance of an object under appropriately provided Extended Light Sources *(ELS)*. The use of ELS for modeling the

shape and reflectance of an object was originally introduced in [11]. We extend their analysis further in the angular frequency domain so that the harmonic images of an object of arbitrary surface materials can be obtained without suffering from aliasing caused by insufficient sampling of its appearance.

The use of ELS has the following advantages. ELS have a radiance distribution that is similar to that of the Gaussian function, and this enables extended sources to function as a low-pass filter when the appearance of an object is sampled under them. From this, we are able to obtain a set of basis images of an object for varying illumination without suffering from aliasing caused by insufficient sampling of its appearance. In addition, ELS can reduce high contrast in image intensities due to specular and diffuse reflection components. This helps avoid saturation so that we are able to observe both specular and diffuse reflection components in the same image taken with a single shutter speed. We have tested our proposed approach based on extended sources with objects of complex appearance that are generally difficult to model using image-based modeling techniques.

The rest of this paper is organized as follows. We briefly review harmonics image representation based on spherical harmonics in Section 2, and discuss the difficulties of obtaining harmonic images of real objects in Section 3. We provide the frequency analysis of ELS in Section 4 and present a method for modeling object's appearance by using ELS in Section 5. Finally, we show experimental results of the proposed method applied to synthetic and real data in Section 6 and present concluding remarks in Section 7.

2 Object Appearance under Variable Illumination

Previous studies have shown that appearance of an object under varying illumination can be well represented with a linear subspace spanned by basis images [14, 15, 1], called harmonic images. In this section, we outline the harmonic image representation that is based on spherical harmonics.

Spherical harmonics define an orthonormal basis over the unit sphere, whose unit vector is represented by the polar coordinate system $\theta, (0 \leq \theta \leq \pi)$ in elevation and $\phi, (0 \leq \phi < 2\pi)$ in azimuth. Then a function $f(\theta, \phi)$ defined over the unit sphere can be expanded as a linear combination of spherical harmonics

$$f(\theta, \phi) = \sum_{l=0}^{\infty} \sum_{m=-l}^{l} F_l^m Y_l^m(\theta, \phi), \qquad (1)$$

and F_l^m are coefficients in its spherical harmonic expansion computed as

$$F_l^m = \int_0^{2\pi} \int_0^{\pi} f(\theta, \phi) Y_l^m(\theta, \phi) \, sin\theta \mathrm{d}\theta \mathrm{d}\phi. \qquad (2)$$

$Y_l^m(\theta, \phi), (l \geq 0, -l \leq m \leq l)$ are spherical harmonics defined as $Y_l^m(\theta, \phi) = N_l^m P_l^m(cos\theta)e^{Im\phi}$, and N_l^m are the

---

[2]Harmonic images have been also used for the purpose of efficient rendering of an object under complex illumination [16, 21].

normalized constants, and $P_l^m(\cdot)$ are the associated Legendre functions of degree l and order m.

2.1 Representing Object Appearance based on Spherical Harmonics

A bidirectional reflectance distribution function (BRDF) characterizes the reflectance property of an object: (θ_i', ϕ_i') and (θ_o', ϕ_o') are incident and reflection directions with respect to the surface normal of the object surface whose local coordinate is denoted by using $'$.

Representing light source distribution $L(\theta, \phi)$ by the global coordinate defined on the unit sphere, the brightness of the object surface is computed as

$$I = \int_0^\pi \int_0^{2\pi} L(\theta, \phi) \rho(M(\theta, \phi), \theta_o', \phi_o') \cos\theta \sin\theta \mathrm{d}\theta \mathrm{d}\phi, \quad (3)$$

where $M(\cdot)$ represents a rotation operator that rotates (θ, ϕ) into the local coordinate.

Considering the appearance changes of an object under variable illumination seen from a fixed viewpoint (θ_o', ϕ_o'), $\rho(M(\theta, \phi), \theta_o', \phi_o') \cos\theta$ can be represented by using a global coordinate $R(\theta, \phi)$. In other words, $R(\theta, \phi)$ represents how much of the incident light from the direction(θ, ϕ) is reflected on the object surface toward the fixed viewpoint (θ_o', ϕ_o'). In the following, $R(\theta, \phi)$ is referred to as the *reflection kernel*.

Since both the light source distribution and the reflection kernel are functions defined on the unit sphere, coefficients L_l^m and R_l^m in their spherical harmonic expansion can be computed from (2). From the orthonormality of spherical harmonics, the surface brightness I in (3) is computed in terms of L_l^m and R_l^m as

$$I = \sum_{l=0}^\infty \sum_{m=-l}^l L_l^m R_l^m. \quad (4)$$

Images containing R_l^m for all pixels, that is, for all corresponding points on the object surface, are called harmonic images [1].

3 Obtaining Harmonic Images via Point Light Sources

While harmonic images are efficient for representing the appearance of objects under varying illumination, it is not so easy to provide harmonic images for various kinds of real objects. Therefore, most of the previously proposed techniques for object recognition and image synthesis provide a reflection kernel of an object from the knowledge of its 3D shape and reflectance properties and synthetically compute the coefficients R_l^m from (2) for all pixels in harmonic images. However, depending on the surface materials of an object, it can be difficult to provide such information.

Recently, we introduced a method to sample the reflection kernel $R(\theta, \phi)$ of an object as an observed brightness of the surface point when the object is illuminated under a light source from the direction (θ, ϕ) [17].[3] In particular, this method made use of the sampling theorem of spherical harmonics for determining a set of lighting directions to properly sample discrete set of the reflection kernel $R(\theta, \phi)$ of an object. The sampling theorem tells us that spherical harmonics transformation of a band-limited reflection kernel with bandwidth B, that is $R_l^m = 0$ ($l \geq B$), can be computed by weighted sums of $4B^2$ sampled function values.

However, the important issue of how to determine the bandwidth of the reflection kernel of a given object still remains to be solved. There is certainly a situation where it is difficult to predict the bandwidth of the reflection kernels of an object, or where only a limited number of samplings of the reflection kernel are obtainable due to the limitation of a hardware set-up used for acquiring input images. In the case where samplings of the reflection kernel of an object are insufficient, the obtained coefficients suffer from aliasing. This leads to undesirable artifacts such as ringing in the reflection kernel reconstructed from those coefficients.

In the next section, we will carefully consider this issue of aliasing and extend the method based on the sampling theorem further for reducing the artifacts due to aliasing, by substituting extended light sources for a point light source to sample the reflection kernel of a real object.

4 Use of Extended Light Sources

Extended light sources (*ELS*) may be constructed by illuminating a spherical diffuser with a point light source as illustrated in Figure 2. The use of ELS brings the following three advantages:

Functioning as a low-pass filter: ELS have a radiance distribution that is similar to that of the Gaussian function. This enables extended sources to function as a low-pass filter when the reflection kernel of an object is sampled under ELS. From this, we are able to model its appearance without suffering from aliasing.

Adjustable bandwidth: The distribution of ELS can be adjusted by changing the distance from the diffuser to a point light source. This enables us to adjust the bandwidth of the ELS in the frequency domain.

Reducing saturation problem: When an object is illuminated by a point light source, image intensities from its specular reflection components often become much greater than those from its diffuse reflection components. Under ELS, the gap between image intensities due to specular and diffuse reflection components are narrowed [11]. This helps avoid saturation, so that we are able to observe both specular and diffuse reflection components in the same image. [4]

In the following, we consider the reflection kernel of an object sampled under ELS.

---

[3]This approach is based on the assumption that a point light has unit radiance and it is sufficiently distant from objects.

[4]The used of the multiplexed illumination proposed in [18] is also effective in reducing this dynamic range problem of capturing both diffuse and specular reflection .
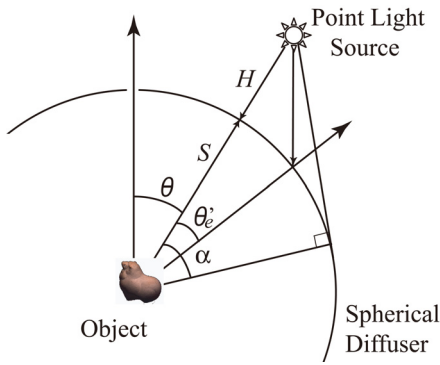
Figure 2. ELS are constructed by a spherical diffuser and a point light source [11].

4.1 Radiance Distribution of ELS

First, the radiance distribution of ELS needs to be provided. The radiance distribution of ELS is symmetric with respect to the point source direction and therefore has no azimuth dependence around the point source direction. Accordingly, the radiance of the inner surface of the diffuser E may be represented as a function of the elevation angle θ'_e, that is $E(\theta'_e, \phi'_e) = E(\theta'_e)$. Here θ'_e represents the elevation angle defined with respect to the direction of the point light source as shown in Figure 2.

Then $E(\theta'_e)$ are computed from the analytic formula derived in [11] as

$$E(\theta'_e) = \frac{CP[(S + H)\cos\theta'_e - S]}{[(S + H - S\cos\theta'_e)^2 + (S\sin\theta'_e)^2]^{\frac{3}{2}}}, \quad (5)$$

where P denotes the radiance of the point source and C is a constant representing the proportionality between the irradiance of the outer surface of the diffuser to the radiance of its inner surfaces. As illustrated in Figure 2, S is the radius of the spherical diffuser, H is the distance from the the diffuser's surface to the point light source.[5]

Here the surface points on the diffuser within the range of $\theta'_e < \alpha$ can receive energy from the point light source, and the effective range α is determined by the relationships between S and H as $\alpha = \cos^{-1}(\frac{S}{S+H})$.

4.2 Reflection Kernel Sampled under ELS

Next, let us consider a reflection kernel $R(\theta, \phi)$ sampled as an observed brightness of an object surface when it is illuminated by ELS whose center is located at the direction (θ, ϕ).

Since radiance of the ELS are distributed over the spherical surface of the diffuser, the modified reflection kernel seen under ELS, denoted as $R'(\theta, \phi)$ is determined by computing the integral of the scene radiance resulting from illumination of the entire surface of the extended source as

$$R'(\theta, \phi) = \int_0^\pi \int_0^{2\pi} R(M_\theta^\phi(\theta'_e, \phi'_e))E(\theta'_e)\sin\theta'_e d\theta'_e d\phi'_e, \quad (6)$$

[5]This formula is based on the condition that the spherical diffuser is ideal and thus incident energy is scattered equally in all directions.
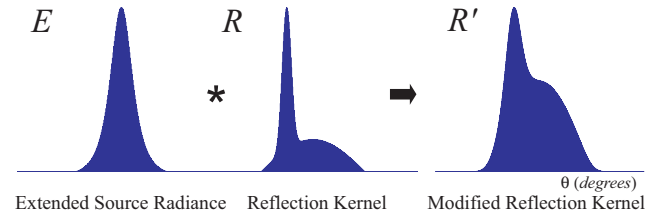
Figure 3. Modified Reflection Kernel obtained by convolving the original reflection kernel $R(\theta, \phi)$ with the distribution of the ELS $E(\theta'_e)$.

where $M_\theta^\phi(\cdot)$ is a rotation operator that rotates the distribution of the ELS $E(\theta'_e)$ so that its center ($\theta'_e = 0$) is located at the direction (θ, ϕ). In other words, the modified reflection kernel $R'(\theta, \phi)$ is determined by convolving the original reflection kernel $R(\theta, \phi)$ with the radiance distribution of the ELS $E(\theta'_e)$ as illustrated in Figure 3.

$R(M_\theta^\phi(\theta'_e, \phi'_e))$ and $E(\theta'_e)$ in (6) can be expanded as a linear combination of spherical harmonics, and (6) is rewritten in terms of spherical harmonics as

$$R'(\theta, \phi) = \sum_{l=0}^\infty \sum_{m=-l}^l R_l^m E_l D_{m,0}^l(\theta)e^{Im\phi}. \quad (7)$$

Mathematical derivation of (7) is shown in the Appendix. R_l^m and E_l represent coefficients in the spherical harmonic expansion of the reflection kernel $R(\theta, \phi)$ and ELS $E(\theta'_e)$ respectively, and the matrix D^l tells us how to compute a rotated spherical harmonic as a linear combination of all the spherical harmonics of the same order l.

The important point to note in (7) is that the modified reflection kernel $R'(\theta, \phi)$ is computed as a product of the coefficient R_l^m and E_l. This indicates that the modified reflection kernel $R'(\theta, \phi)$ is band-limited with the lower bandwidth between $R(\theta, \phi)$ and $E(\theta'_e)$. Fortunately, it is not difficult to adjust the bandwidth of the ELS.

4.3 Adjusting Bandwidth of ELS

As has been noted above, ELS used in our approach have a distribution similar to that of the Gaussian function, and their distribution and effective range α are determined by the radius S of a spherical diffuser and the distance H from the diffuser surface to a point light source as shown in (5). In other words, the closer the point light source is positioned to the diffuser, the narrower its range α becomes. This property of Extended Light Sources enables us to specify their bandwidth.

The Fourier transform of the Gaussian function is known to lead to another Gaussian function in the frequency domain. In addition, the standard deviation σ_f of the Gaussian function in the frequency domain is known to become inversely proportional to the standard deviation σ_s of the Gaussian function in the spatial domain. That is $\sigma_f = \frac{1}{\sigma_s}$. Similarly,

Spatial domain | Frequency domain
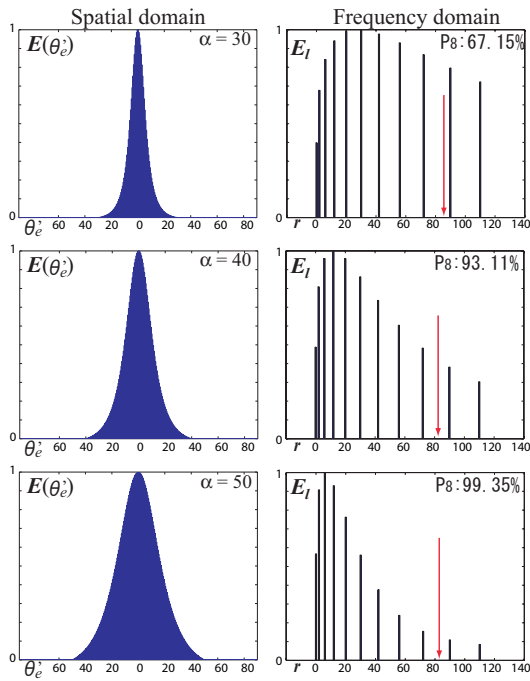
Figure 4. Distribution of ELS (left: spatial domain, right: frequency domain).

we can safely say that the Gaussian function defined on the unit sphere also results in a half-Gaussian distribution of the coefficients, that is a Gaussian distribution with a half range, in its spherical harmonic expansion.

To see how bandwidth of ELS changes depending on their α values, we synthetically provide several radiance distributions of ELS with different α values from (5). The coefficients E_l and the corresponding α of those extended sources are shown in Figure 4. In this figure, spherical harmonic coefficients for given degree l and order m are represented using a single index $r = l^2 + l + m$. The horizontal axis represents the index r, and the vertical axis represents the computed coefficients E_l.

In each graph in this figure, the left side of a red arrow corresponds to the coefficients up to the degree $l = 8$. The energy captured by spherical harmonics up to the degree $l = 8$, denoted as P_8 are also computed by sums of the squares of their respective coefficients divided by the total squared energy of the transformed function. In this figure, we clearly see that P_8 becomes closer to 100% as their α values increase from 30 to 50 degrees. Especially in the case of $\alpha = 50$ degrees, more than 99% of the total energy is captured by the spherical harmonics up to the degree $l = 8$, so it is reasonable to assume that the extended source generated with $\alpha = 50$ degrees is band limited with bandwidth $l = 8$. As shown in this example, the bandwidth of ELS can be set by adjusting their effective range α.

5 Modeling Appearance by using ELS

Based on the analysis provided in the previous section, we propose a novel scheme for sampling the reflection kernel of

an object by ELS with a properly adjusted range α. Here we employ the efficient sampling theorem in spherical harmonics proposed in [9].

This sampling theorem tells us that spherical harmonics transformation of a band-limited function with bandwidth B ($F_l^m = 0$ ($l \geq B$)), can be computed by weighted sums of $2B^2 - B$ sampled function values based on Gaussian quadrature [13] as

$$F_l^m = \frac{2\pi}{2B-1} \sum_{j=0}^{B-1} \sum_{k=0}^{2B-2} w_j f(\theta_j, \phi_k) Y_l^m(\theta_j, \phi_k), \quad (8)$$

where the weights w_j are weights of Gaussian quadrature, θ_j are Gaussian nodes in $\cos\theta$, and $\phi_k = \frac{2\pi k}{(2B-1)}$ are equally sampled in azimuth [9, 12].

In order to avoid aliasing caused by insufficient sampling of the appearance of an object, we observe its reflection kernel under ELS whose bandwidth is properly adjusted to B. By doing so, the modified reflection kernel $R'(\theta, \phi)$ of the object sampled under the ELS also becomes band-limited with the same bandwidth B as the ELS, and this enables us to model the appearance of the object from a set of sampled $R'(\theta_j, \phi_k)$ without suffering from aliasing caused due to insufficient sampling of the original reflection kernel $R(\theta, \phi)$.

6 Experimental Results: Synthetic and Real

6.1 Synthetic Data

The reflection kernel $R(\theta, \phi)$ of several surface materials are synthetically provided based on the Ward isotropic reflection model [22] with known reflection parameters as shown in Table 1.[6] Here the surface normal and viewing direction for the reflection kernel are set at the direction ($\theta_n = 0, \phi_n = 0$) and ($\theta_o = 45, \phi_o = 0$) respectively.

The ELS used in this experiment are generated with $\alpha = 50$ degrees whose bandwidth is equivalent to $B = 9$. This makes the modified reflection kernel $R'(\theta, \phi)$ band-limited with $B = 9$. Accordingly, the spherical harmonic coefficients $R_l'^m$ of the band-limited function $R'(\theta, \phi)$ were obtained from a properly sampled discrete set of the function values (153 samplings for $B = 9$ in (8)).

The right columns in Figure 5, and 6 show the obtained reflection kernel for glossy gray paper and lightly brushed aluminum surfaces respectively. b) shows computed coefficients $R_l'^m$, and d) and f) show the distribution of $R'(\theta, \phi)$ reconstructed from the obtained $R_l'^m$ in (1) up to the degree $l = 8$.[7]

For reference, the left columns of these figures show the coefficients and distribution of the original reflection kernel $R(\theta, \phi)$. a) shows its coefficients computed from 100000

---

[6] K_d and K_s are constants for the diffuse and specular reflection components, and σ is the standard deviation of the surface slope.

[7] d) shows $R'(\theta, \phi)$ scanned in the line of $\{\theta | 0 \leq \theta \leq \pi/2\}$, $\{\phi | 0$ or $\pi\}$, and f) shows the upper half of the reflection kernel visualized in a polar coordinate system with radius indicating $\{\theta | 0 \leq \theta \leq \pi/2\}$, and angle indicating $\{\phi | 0 \leq \phi < 2\pi\}$.

Table 1. Reflection parameters.

Material	k_d	k_s	σ
glossy gray paper	.29	.083	.082
lightly brushed aluminum	.15	.19	.088

samplings of $R(\theta, \phi)$, and c) and e) show its distribution computed by substituting the reflection parameters into the Ward reflection model.

Comparing a) with b), while the magnitude of the coefficients is different because of the multiplication with the coefficients of the ELS whose distribution is similar to that of a half Gaussian function, the recovered R'^m_l go up and down in the same manner as R^m_l if we see their distributions locally. In Figure 7 a) and b), we also provide the low-frequency appearance of the original reflection kernel for reference by substituting the coefficients R^m_l up to degree $l = 8$ into (1). In other words, all coefficients with the index $l > 8$ of R^m_l are truncated in this case. Comparing f) with the low-frequency appearance of the original reflection kernel in Figure 7 a), the modified reflection kernel reconstructed by our method provides a good representation of the low-frequency appearance of the original reflection kernel, although high-frequency appearance such as the specular peak in e) is blurred due to the approximation of the original reflection kernel up to the degree $l = 8$.

It is worth noting that almost no undesirable artifacts appear in the reconstructed reflection kernel $R'(\theta, \phi)$ in f). This shows that the proposed method succeeded in computing the coefficients R'^m_l of the modified reflection kernel from the discrete 153 samplings of $R'(\theta, \phi)$ without suffering from aliasing due to insufficient sampling of its appearance. In contrast, as Westin et al. pointed out in [23], simply truncating all coefficients R^m_l with $l > 8$ resulted in undesirable artifacts such as ringing in the reconstructed reflection. This ringing is called the Gibbs phenomenon and is shown in Figures 7 a) and b).

In order to avoid the Gibbs phenomenon, Westin et al. progressively reduced the magnitude of the coefficients according to a half Gaussian distribution of an empirically determined width. Fortunately, the coefficients of the ELS used in our method have a distribution that is similar to that of a half Gaussian distribution, as shown in Figure 4. It follows from this that the use of ELS is desirable not only as a method of modifying the original reflection kernel to be band-limited, but also for reducing the number of artifacts caused by the truncation of the coefficients with index $l \geq B$ of the original reflection kernel. [8]

6.2 Real Data

Real images of abalone shellfish were taken under the physically constructed ELS apparatus shown in Figure 1.

---

[8] $R'(\theta, \phi)$ is computed as a product of R^m_l, E_l, and D^l in (7). Since E_l and D^l are computable numbers, we are able to recover R^m_l of the original reflection kernel from the set of modified reflection kernel $R'(\theta, \phi)$ if necessary.
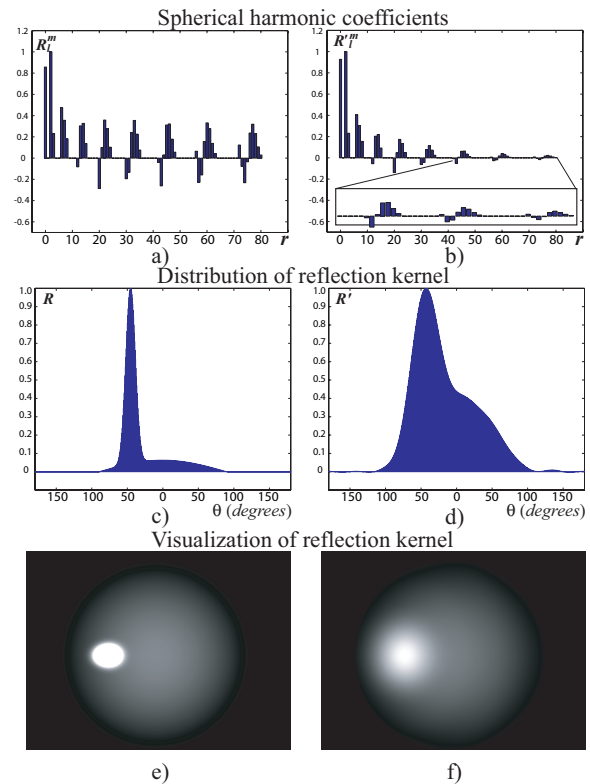
Figure 5. Glossy gray paper : original reflection kernel (left), recovered modified reflection kernel (right).
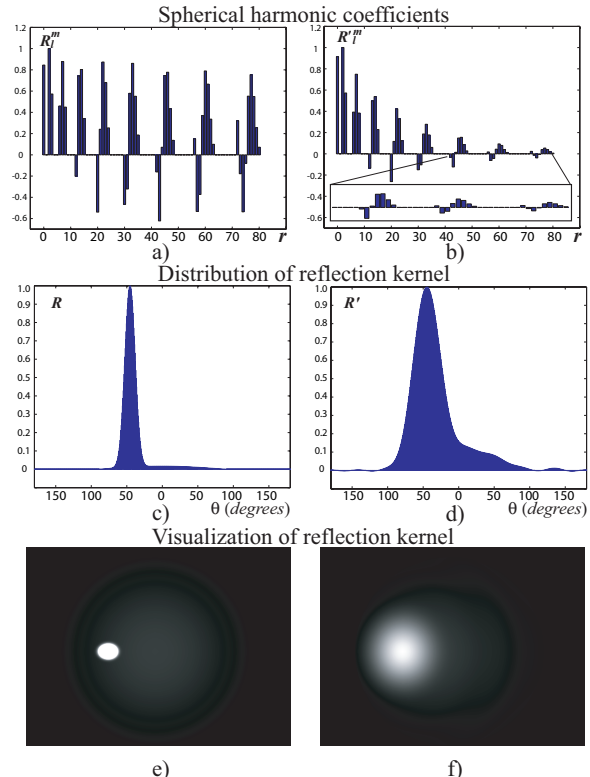
Figure 6. Lightly brushed aluminum : original reflection kernel (left), recovered modified reflection kernel (right).

glossy gray paper

lightly brushed aluminum

a)   b)
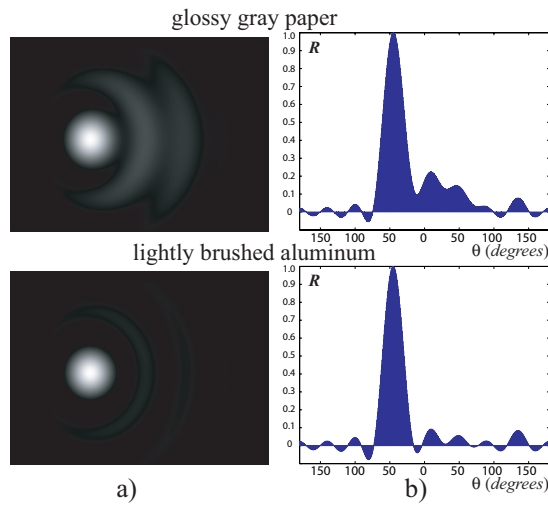
Figure 7. Reconstructed reflection kernel from the coefficients R_l^m of the original reflection kernel up to the degree $l = 8$.

Abalone shellfish is famous for its interesting structural colors which alter greatly depending on viewing direction and illumination conditions. In this set-up, 9 halogen lamps were positioned at Gaussian nodes in elevation, and an array of these light sources were mounted on a turntable and rotated around the spherical diffuser (an acrylic globe with a diameter of 35cm) by $\phi_k = \frac{2\pi_k}{(18-1)}, (k = 0, \ldots, 16)$ degrees in azimuth. Here the number of point light sources in elevation indicates that a modified reflection kernel has to be bandlimited with $B = 9$. Accordingly the distance between the diffuser and the point light sources was adjusted so that the bandwidth of the constructed ELS was set to $B = 9$.

In total, 153 input images of the abalone shellfish were taken to sample its reflection kernel at each grid point (θ_j, ϕ_k). Then coefficients R'^m_l of this reflection kernel were computed up to the degree $l = 8$ by substituting the observed reflection kernel $R'(\theta_j, \phi_k)$ into (8). The first nine harmonic images obtained by our method are shown in Figure 8 (a).

Figure 8 (b) shows the appearance of the abalone shellfish synthesized from (4) under natural illumination conditions provided as high-dynamic range light probe measurements by [2]. In this figure, the synthesized appearance of the abalone shellfish significantly changes depending on the characteristics of the given illumination distributions, and this shows that the complex appearance of its structural colors are well represented by a set of basis images obtained by our method.

In addition, the synthesized appearance of the shellfish is compared with its real appearance as seen under a normal lighting condition in our laboratory in Figure 1.[9] In this figure, the synthesized appearance highly resembles the real image. As has been noted before, in the case of a highly specular surface, image intensities from specular reflection components tend to be much greater than those from diffuse reflection components. This is the reason why image intensities in

---

[9]Coefficients L_l^m of this lighting condition are computed from an omni-directional image of the scene taken by a camera with a fish-eye lens.

$(l,m) = (0, 0)$ $(0, -1)$ $(1, 1)$ $(1, 1)$ $(2, -2)$

$(2, -1)$ $(2, 0)$ $(2, 1)$ $(2, 2)$
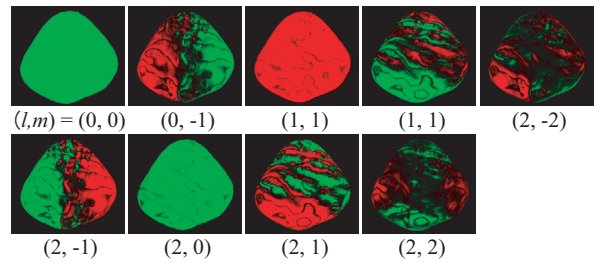
(a) Obtained harmonic images: positive values are shown in green; negative values are shown in red.
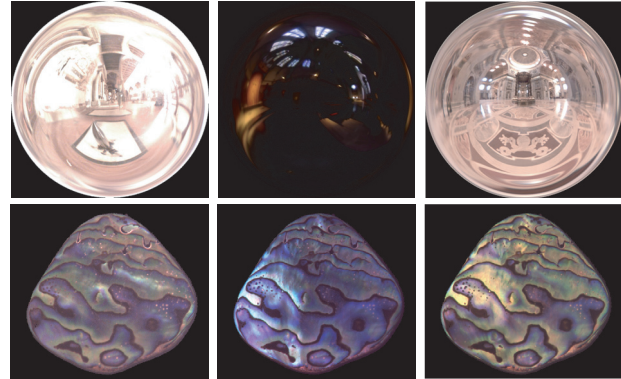
(b) Synthesized images under natural Illumination conditions

Figure 8. (a) Obtained harmonic images. (b) Synthesized images under natural illumination conditions.

the real image become saturated in some specular regions.

In general, the limited dynamic range of an image taken with one shutter speed makes it difficult to model the appearance of highly specular surfaces. In contrast, the use of ELS contributes to reduce the high contrast between image intensities from both specular and diffuse components. This helps us to observe and model the appearance of highly specular surfaces from images taken at a single shutter speed.

7   Conclusions

In this paper we have demonstrated the effectiveness of using Extended Light Sources (ELS) for modeling the appearance of an object under varying illumination. The use of ELS for modeling the appearance of objects has the following advantages: (1) ELS have the ability to function as a low-pass filter for sampling objects' appearance, so basis images of an object can be obtained without suffering from aliasing caused by insufficient sampling of its reflection kernel, (2) ELS can reduce the high contrast between image intensities from both specular and diffuse components. This helps us observe and model the appearance from images taken at a single shutter speed, and (3) ELS can minimize undesirable artifacts resulting from the truncation of spherical harmonic coefficients of higher degrees. These advantages help provide basis images of an object from a limited number of samplings of its appearance. Our method can adequately synthesize the appearance of an object up to a certain frequency. However, objects of high bandwidth such as a mirror illuminated by a point

light source are difficult to be adequately modeled. A future research direction of this work would be to integrate other modeling techniques with the objective of recovery of an object original reflection kernel. Also, it would be interesting to investigate the potential of other types of light sources serving as a low-pass filter when the appearance of an object is sampled under them.

Acknowledgments

References

[1] R. Basri and D. Jacobs, "Lambertian Reflectance and Linear Subspaces," *Proc. IEEE Intl. Conf. Computer Vision 01*, pp.383-389, 2001.

[2] P. Debevec, "Rendering synthetic objects into real scenes: Bridging traditional and image-based graphics with global illumination with high dynamic range photography," *Proc. SIGGRAPH 98*, pp. 189-198, 1998.

[3] R. Epstein, P. Hallinan, and A. Yuille, "5+/-2 eigenimages suffice: An empirical investigation of low-dimensional lighting models," *Proc. IEEE Workshop on Physics-Based Modeling in Computer Vision*, pp. 108-116, 1995.

[4] A. Georghiades, D. Kriegman, and P. Belhumeur, "Illumination cones for recognition under variable lighting: Faces," *Proc. IEEE Conf. Computer Vision and Pattern Recognition*, pp. 52-59, 1998.

[5] A. Georghiades, D. Kriegman, and P. Belhumeur, "From few to many: Generative models for recognition under variable pose and illumination," *IEEE Trans. Pattern Analysis and Machine Intelligence*, vol. 23, no. 6, pp. 643-660, 2001.

[6] P. Hallinan, "A low-dimensional representation of human faces for arbitrary lighting conditions," *Proc. IEEE Conf. Computer Vision and Pattern Recognition*, pp. 995-999, 1994.

[7] K. C. Lee, J. Ho, and D. Kriegman, "Nine points of light: Acquiring subspaces for face recognition under variable lighting," *Proc. IEEE Conf. Computer Vision and Pattern Recognition 01*, pp.519-526, 2001.

[8] T. Malzbender, D. Gelb, and H. Wolters, "Polynomial texture maps," *Proc. SIGGRAPH 01*, pp. 519-528, 2001.

[9] M. J. Mohlenkamp, "A Fast Transform for Spherical Harmonics," *J. Fourier Analysis and Applications*, vol. 5(2/3), pp.159-184, 1999.

[10] H. Murase and S. Nayar, "Visual learning and recognition of 3-D objects from appearance," *Int. J. Computer Vision*, vol. 14, no. 1, pp. 5-24, 1995.

[11] S. K. Nayar, K. Ikeuchi, and T. Kanade, "Determining shape and reflectance of hybrid surfaces by photometric sampling," *IEEE Trans. Robotics and Automation*, vol. 6, no. 4, pp. 418-43, 1990.

[12] T. Okabe, I. Sato, and Y. Sato, "Spherical Harmonics vs. Haar Wavelets: Basis for Recovering Illumination from Cast Shadows," *Proc. IEEE Conf. Computer Vision and Pattern Recognition*, pp.I-50-57, 2004.

[13] W. H. Press, B. P. Flannery, S. A. Teukolsky, W. T. Vetterling, *Numerical Recipes in C: The Art of Scientific Computing*, Cambridge University Press, Cambridge, 1988.

[14] R. Ramamoorthi and P. Hanrahan, "A signal-procession framework for inverse rendering", *Proc. SIGGRAPH 01*, pp.117-128, 2001

[15] R. Ramamoorthi and P. Hanrahan, "On the relationship between radiance and irradiance: Determining the illumination from images of a convex lambertian object," *J. Optical Society of America A*, vol. 18, no. 10, pp. 2448-2459, 2001.

[16] R. Ramamoorthi and P. Hanrahan, "An efficient representation for irradiance environment maps," *Proc. SIGGRAPH 01*, pp. 497-500, 2001.

[17] I. Sato, T. Okabe, Y. Sato, and K. Ikeuchi, "Appearance sampling for obtaining a set of basis images for variable illumination," *Proc. IEEE Int'l Conf. Computer Vision*, pp. 800-807, 2003.

[18] Y. Schechner, S. Nayar, and P. Belhumeur, "A Theory of Multiplexed Illumination," *Proc. IEEE Int'l Conf. Computer Vision*, pp. 808-815, 2003.

[19] K. Shim and T. Chen, "Efficient representation of lighting patterns for image-based relighting," *Proc. Picture coding symposium*, 2004.

[20] A. Shashua, "On photometric issues in 3D visual recognition from a single image," *Int. J. Computer Vision*, vol. 21, pp. 99-122, 1997.

[21] P. Sloan, J. Kautz, and J. Snyder, "Precomputed radiance transfer for real-time rendering in dynamic, low-frequency lighting environments," *SIGGRAPH 02*, pp. 527-536, 2002.

[22] G. J. Ward, "Measuring and modeling anisotropic reflection," *Proc. SIGGRAPH '92*, pp. 265-272. 1992.

[23] S. Westin, J. Arvo, K. Torrance, "Predicting Reflectance Functions from Complex Surfaces, " *Proc. SIGGRAPH '92*, pp. 255-264, 1992.

[24] A. Yuille, D. Snow, R. Epstein, and P. Belhumeur, "Determining generative models of objects under varying illumination: Shape and albedo from multiple images using SVD and integrability," *Int. J. Computer Vision*, vol. 35, no. 3, pp. 203-222, 1999.

[25] L. Zhao and Y. Yang, "Theoretical analysis of illumination in PCA-based vision systems," *Pattern Recognition*, vol. 32, pp. 547-564, 1999.

Appendix

A modified reflection kernel $R'(\theta, \phi)$ is described by

$$R'(\theta,\phi) = \int_0^\pi \int_0^{2\pi} R(M_\theta^\phi(\theta_e', \phi_e')) E(\theta_e') \sin\theta_e' \mathrm{d}\theta_e' \mathrm{d}\phi_e', \qquad (9)$$

$R(M_\theta^\phi(\theta_e', \phi_e'))$ and $E(\theta_e')$ can be expanded as a linear combination of spherical harmonics:

$$E(\theta_e') = \sum_{n=0}^\infty E_n Y_n^0(\theta_e') \qquad (10)$$

$$R(M_\theta^\phi(\theta_e', \phi_e')) = \sum_{l=0}^\infty \sum_{m=-l}^l R_l^m Y_l^m(M_\theta^\phi(\theta_e', \phi_e')), \quad (11)$$

where R_l^m and E_n denote coefficients in their spherical harmonic expansion. Then a rotation formula for spherical harmonics is given in [14] as $Y_l^m(M_\theta^\phi(\theta_e', \phi_e')) = \sum_{m'=-l}^l D_{m,m'}^l(\theta) e^{Im\phi} Y_l^{m'}(\theta_e', \phi_e')$, where the term $e^{Im\phi}$ considers the rotation about ϕ, and the matrix D^l tells us how to compute a rotated spherical harmonic as a linear combination of all the spherical harmonics of the same order l.
Substituting (10) and (11), (9) becomes

$$R'(\theta,\phi) = \sum_{n=0}^\infty \sum_{l=0}^\infty \sum_{m=-l}^l \sum_{m'=-l}^l R_l^m E_n D_{m,m'}^l(\theta) e^{Im\phi} \qquad (12)$$

$$\int_0^\pi \int_0^{2\pi} Y_l^{m'}(\theta_e', \phi_e') Y_n^0(\theta_e') \sin\theta_e' \mathrm{d}\theta_e' \mathrm{d}\phi_e'.$$

Then the orthonormality of the spherical harmonics tells us $\int_0^\pi \int_0^{2\pi} Y_l^{m'}(\theta_e', \phi_e') Y_n^0(\theta_e') \sin\theta_e' \mathrm{d}\theta_e' \mathrm{d}\phi_e' = \delta_{ln}\delta_{m'0}$, and therefore

$$R'(\theta,\phi) = \sum_{n=0}^\infty \sum_{l=0}^\infty \sum_{m=-l}^l \sum_{m'=-l}^l R_l^m E_n D_{m,m'}^l(\theta) e^{Im\phi} \delta_{ln}\delta_{m'0}.$$

$$(13)$$

Finally, from the characteristics of Kronecker delta ($\delta_{ij} = 1$ if $i = j$, and $\delta_{ij} = 0$ if $i \neq j$), the modified reflection kernel is obtained

$$R'(\theta,\phi) = \sum_{l=0}^\infty \sum_{m=-l}^l R_l^m E_l D_{m,0}^l(\theta) e^{Im\phi}. \qquad (14)$$